Production of the "$K^- pp$"-like structure in the $d(\pi^+, K^+)$ reaction at 1.69 GeV/c

Tomofumi Nagae*

Kitashirakawa, Sakyo-ku, Kyoto 606-8502, Japan
Department of Physics, Kyoto University

Abstract

We have investigated the $\pi^+ + d \to K^+ + X$ reaction at 1.69 GeV/c at the hadron experimental hall of J-PARC. Systems with baryon number $B = 2$ and strangeness $S = -1$ are produced in this reaction. Owing to the very wide momentum acceptance of the spectrometer, we were able to search from the ΛN threshold to above the $\bar{K}NN$ threshold, which covers the energy region where the $K^- pp$ bound state and/or the $\Sigma(1385)N$ bound state could show up.

We observed a significant shift of the quasi-free $\Sigma(1385)/\Lambda(1405)$ production peak by approximately 30 MeV to the lighter mass side. Further, with the coincidence of two protons in the final state, a broad bump structure was observed with a mass and width of $2275^{+17}_{-18}(stat)^{+21}_{-30}(syst)$ MeV/c^2 and $162^{+87}_{-45}(stat)^{+66}_{-78}(syst)$ MeV coming from the $K^- pp \to \Sigma^0 + p$ decay.

Keywords: Kaonic Nuclei, $\Lambda(1405)$, $\bar{K}N$ Interaction

1. Introduction

In the baryon number $B = 2$ systems made of nucleons, there is one bound state of the deuteron with isospin $I = 0$ and spin-parity $J^P = 1^+$. The properties of the deuteron gave us useful information on nuclear force. Namely, the finite value of the quadrupole moment comes from the tensor force due to one pion exchange, which mixes the $S-$wave and $D-$wave components.

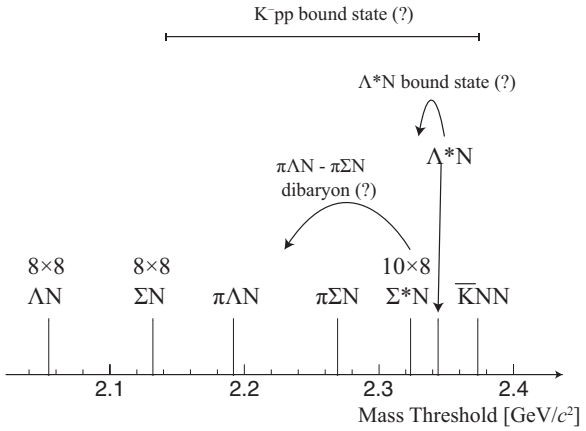

Figure 1: Various threshold mass values with Baryon number $B = 2$ and Strangeness $S = -1$ systems up to $\bar{K}NN$.

*Corresponding author
Email address: nagae@scphys.kyoto-u.ac.jp (Tomofumi Nagae)

When we look into the baryon number $B = 2$ systems with strangeness $S = -1$ (Fig. 1), we could have two kinds of systems with octet baryons **8**: Λ- and Σ-hypernuclei. The threshold masses for ΛN and ΣN are 2.05 GeV/c^2 and 2.13 GeV/c^2, respectively.

However, we know that there are no bound states in the ΛN system. The lightest Λ-hypernucleus ever observed is hyper-triton, ${}^{3}_{\Lambda}$H, with a binding energy of 0.13±0.05 MeV and spin-parity $J^P = \frac{1}{2}^+$ [1]; $B = 3$ and $S = -1$.

Further, there are no Σ bound states in ΣN [2]. The lightest and almost unique bound state observed is ${}^{4}_{\Sigma}$He [3]; $B = 4$ and $S = -1$. It is understood that the isospin dependence of the ΣN interactions make this state unique [4, 5].

Above these, there are pion production thresholds of $\pi\Lambda N$ and $\pi\Sigma N$ at 2.19 GeV/c^2 and 2.27 GeV/c^2, respectively. In much heavier systems, we have hyperon resonances (Σ^* and Λ^*): namely, Σ(1385) with $J^P = \frac{3}{2}^+$ and Λ(1405) with $J^P = \frac{1}{2}^-$. The mass and width for the former resonance are approximately 1383 MeV/c^2 and 36 MeV, and 1405 MeV/c^2 and 50.5 MeV for the latter. Thus, these thresholds of $\Sigma(1385)N$ and $\Lambda(1405)N$ are 2.32 GeV/c^2 and 2.34 GeV/c^2.

The Σ(1385) belongs to the decuplet baryons, such as Δ(1232)s, with spin-parity $J^P = \frac{3}{2}^+$ and isospin $I = 1$, which mainly decays into $\Lambda\pi(87.0 \pm 1.5)\%$ and $\Sigma\pi(11.7 \pm 1.5)\%$. In the dibaryonic system of the $\Sigma(1385)N$, the existence of a $\pi\Lambda N$-$\pi\Sigma N$ dibaryon as a bound state of the $\Sigma(1385)N$ with $I = \frac{3}{2}$ and $J^P = 2^+$ near the $\pi\Sigma N$ threshold is suggested [6].

The Λ(1405) has spin-parity $J^P = \frac{1}{2}^-$ [7]. Owing to the isospin, it decays to $\Sigma\pi(100\%)$. The Λ(1405) mass is small compared with a naive quark model prediction. Therefore, there has been a discussion on the structure of the Λ(1405), and specifically, whether it is an ordinary baryon with three constituent quarks or a $\bar{K}N$ molecule. A recent lattice QCD calculation suggests the latter is the case [8]. There could be a $\Lambda(1405)N$ bound state with $I = \frac{1}{2}, J^P = 0^-$ depending on the $\Lambda(1405)N$ interaction [9].

Finally, just above the threshold of the $\Lambda(1405)N$ at 2.34 GeV/c^2, we have the $\bar{K}NN$ threshold at 2.37 GeV/c^2. It sits on above 49 MeV and 27 MeV from the $\Sigma(1385)N$ and $\Lambda(1405)N$ thresholds, respectively. Since there is a strong attraction in the $I = 0$ $\bar{K}N$ channel, a bound state of $\bar{K}NN$ with $I = \frac{1}{2}, J^P = 0^-$, which is called "$K^-pp$", is predicted to exist [10]. The "K^-pp" binding energy was theoretically estimated to be approximately 10-20 MeV for energy-dependent chiral interactions and 40-90 MeV for energy-independent $\bar{K}N$ interactions [11]. Assuming the Λ(1405) is a molecule of $\bar{K}N$, it is difficult to discriminate the $\Lambda(1405)N$ bound state and the "K^-pp" bound state because they have the same quantum numbers.

The experimental status of the K^-pp is summarized in a review talk in the HYP2015 conference [12]. Here, I briefly mention some of the results. The first experimental evidence for the existence of the "K^-pp" bound state was reported by the FINUDA collaboration in the $(K^-_{stop}, \Lambda p)X$ reaction on ^{6}Li, ^{7}Li, and ^{12}C targets [13]. A binding energy and width of $115^{+6}_{-5}(\text{stat.})^{+3}_{-4}(\text{syst.})$ MeV and $67^{+14}_{-11}(\text{stat.})^{+2}_{-3}(\text{syst.})$ MeV were reported. In the $p + p \to K^+\Lambda p$ reactions, the DISTO group found a signal with a binding energy of 103±3(stat.)±5(syst.) MeV and a width of 118±8(stat.)±10(syst.) MeV at an incident proton energy of 2.85 GeV [14]. They also reported there were no signals at 2.5 GeV [15]. The HADES collaboration measured the same reaction at much higher energy of 3.5 GeV, and found no signal [16]. The OBELIX group reported a narrow peak structure in the invariant mass of the $p\pi^- - p$ coming from Λp in the $\bar{p}{}^4$He annihilations at rest [17, 18]. It has a width of <33.9±6.2 MeV and the binding energy of 151.0±3.2(stat.)±1.2(syst.) MeV. There are recent inclusive measurements in the $d(\gamma, K^+\pi^-)$ reaction at SPring-8/LEPS [19] and in the ${}^3\text{He}(K^-, n)$ reaction in the J-PARC E15 [20]. Both measurements were unable to observe the deeply bound signal, and only production cross-section upper limits were set.

Three bound states of $B = 2$, $S = -1$ systems, $\Sigma(1385)N$, $\Lambda(1405)N$, and $\bar{K}NN$, can be located anywhere in between the ΣN and the $\Sigma(1385)N$ thresholds, if they exist. Of course, they are particle-unstable and decay into ΛN, ΣN, $\pi\Lambda N$, and $\pi\Sigma N$ if allowed. The decay width may be 40-100 MeV. In the case of K^-pp, the main decay mode is expected to be $\pi\Sigma N$ mode unless the binding energy is so large that this decay mode is energetically forbidden, which would be the case for the binding energy greater than 100 MeV.

These are the systems of $B = 2$, $S = -1$ between the ΛN threshold and the $\bar{K}NN$ threshold. The properties of hyperons and hyperon resonances are rather well known. However, their behaviors in nuclear media have not been investigated yet. Before considering the new system, let us look back at the systems of $B = 2$, $S = 0$ such as ΔN and $\Delta\Delta$.

The first excited state of the nucleon is the Δ resonance at a mass of 1232 MeV/c^2 and a width of 120 MeV with spin $\frac{3}{2}$ and isospin $\frac{3}{2}$, which belongs to baryon decuplet **10** in flavor $SU(3)$. The properties of Δ in nuclei have been investigated by exciting it with medium-energy pion beams in so-called Pion Factories such as TRIUMF,

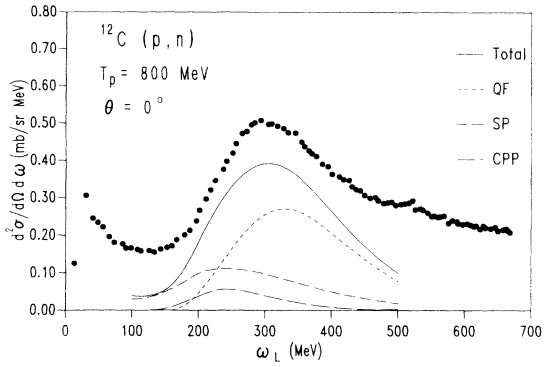

Figure 2: Decomposition of the zero-degree cross-section into partial cross-sections for the ^{12}C(p, n) reaction at 800 MeV. The contributions are due to quasifree Δ decay (QF), Δ spreading (SP), and coherent pion production (CPP). Taken form Ref. [24].

LAMPF, and PSI. The propagations of Δ in nuclei were described in the framework of the $\Delta - hole$ model [21]. The Δ escapes from a nucleus ($\Delta N \rightarrow \Delta N$, $\Delta \rightarrow \pi N$) or is absorbed in a nucleus ($\Delta N \rightarrow NN$). The Δ is broadened due to the latter conversion process and the spectrum shape is modified. In fact, there were several experimental observations in the Δ production reactions that the Δ mass was shifted to the lower mass side by ∼70 MeV in inclusive (^{3}He, t) and (p, n) reactions [22]. In contrast to these hadronic excitations of Δ, almost no shift was observed in electromagnetic excitations such as photo-absorption reactions and inelastic electron scattering. Also, it was reported that when the Δ production was identified with the $\Delta \rightarrow p\pi^-$ decay(quasi-free Δ production), there was no shift [23]. From the ∼70 MeV shift, approximately 40 MeV was explained by a trivial nuclear Fermi motion effect, while the remaining 30 MeV was important in the hadronic excitations and could be explained as the difference between the spin-longitudinal response and the spin-transverse response. By inspecting the decay modes, this shift component was further recognized as the coherent pion production process (Fig. 2) [24, 25] in which a Δ is excited with a nucleon hole and the nucleon from the $\Delta \rightarrow \pi N$ decay fills the nucleon hole emitting only a pion. The nucleus is left in its ground state after the process. This is nothing but pion elastic scattering, while a virtual pion is impinged in the case of the (p, n) reaction [25]. In the theoretical calculation, it was shown that the coherent pion process is dominated by the longitudinal component.

At much higher energies, we can further excite the ΔΔ state with $\Delta N \rightarrow \Delta\Delta$. Here, strong attraction between the $\Delta - \Delta$ is expected in several theoretical models predicting dibaryon states with $B = 2$, $J^P = 3^+$, and $I = 0$ [26, 27]. The WASA@COSY collaboration measured the energy dependence of the $pn \rightarrow d\pi^0\pi^0$ reaction and analyzing power, which clearly indicates a resonance structure in the $^3D_3$ partial wave at a mass of approximately 2.38 GeV/c^2 and width of approximately 70 MeV [28, 29]. This is good evidence for the ΔΔ dibaryon resonance with I(J^P)=0(3^+).

2. Experimental Setup of J-PARC E27

We have performed the J-PARC E27 experiment to investigate the $B = 2, S = -1$ dibaryonic systems, aiming for the "K^-pp" bound state, in the $\pi^+ + d \rightarrow K^+ + X$ reaction at 1.69 GeV/c. In 2012, the measurement was performed at the K1.8 beam line [30] in the hadron experimental hall, using a high-intensity pion beam of $\sim 3 \times 10^6$ π^+s per 6 s spill cycle. At this incident beam momentum, not only the ground-state hyperons of Λ(1116) and Σ(1190), but also the hyperon resonances of Λ(1405) and Σ(1385) are produced. In fact, the $\pi^- + p \rightarrow K^0 + \Lambda(1405)$ reaction at 1.69 GeV/c is one of the few reactions in which the line shape of the Λ(1405) was clearly observed [31]. This is the reason for setting the incident momentum at 1.69 GeV/c.

In this reaction, a possible "K^-pp" bound state production mechanism is suggested [32] to feed the K^-pp through the Λ(1405) as a doorway: namely $\Lambda^* + p \rightarrow$"$K^-pp$" after the Λ^*(Λ(1405) in off-mass shell) production via $\pi^+ + n \rightarrow K^+ + \Lambda^*$. Considering the large recoil momentum of the Λ(1405), however, the sticking probability of the Λ(1405) would not be so high [32]. Most of the Λ(1405) will escape from the deuteron without rescattering. Thus, we need

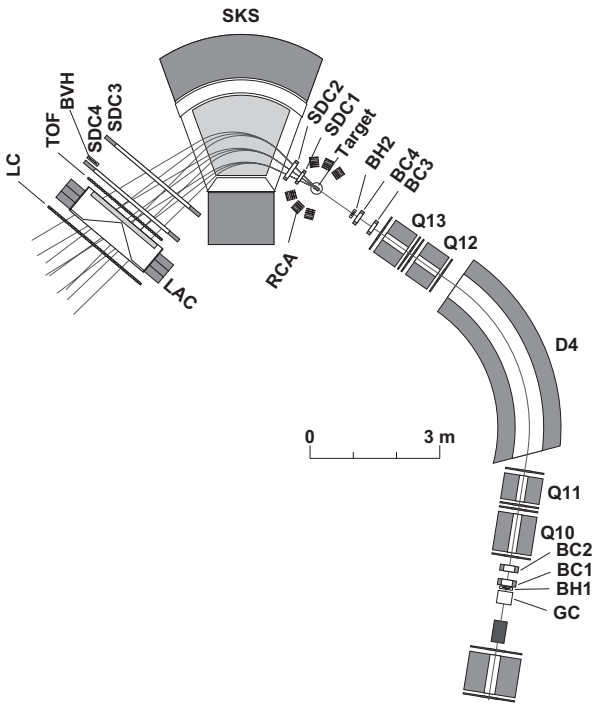

Figure 3: Schematic view of the E27 experimental setup [33]. The K1.8 beam line spectrometer has four tracking detectors, BC1-4, and two trigger hodoscopes, BH1-2. The SKS spectrometer also has four tracking detectors, SDC1-4, and three kinds of trigger detectors, TOF, LC (Lucite Cherenkov), and LAC (Large Aerogel Cherenkov).

some coincidence to enhance the signal to noise ratio. Assuming we have enough branches for non-mesonic decays such as "$K^- pp$"$\rightarrow \Lambda + p/\Sigma^0 + p$, we can expect that rather high-momentum protons ($\gtrsim$ 250 MeV/c) will be emitted in a wide angular range. We have prepared a range counter system for this purpose.

Figure 3 shows a schematic view of the E27 experimental setup [33]. The incident pion momentum was analyzed with a K1.8 beam line spectrometer composed of four quadrupole and one dipole(Q10, Q11, D4, Q12, and Q13) magnets in the last section of the beam line. A liquid deuterium target of 1.99 g/cm^2 thickness was used for the $d(\pi^+, K^+)$ reaction at 1.69 GeV/c, and a liquid hydrogen target of 0.85 g/cm^2 for $p(\pi^+, K^+)$ reactions at 1.58 and 1.69 GeV/c for calibration. The SKS spectrometer was used for the momentum analysis of scattered K^+ covering the scattering angle between 2° and 16° in the laboratory system. It has a wide momentum acceptance of 0.8–1.3 GeV/c with the central magnetic field of 2.36 T. Thereby, we could investigate the $B = 2, S = -1$ systems of the ΛN, ΣN, $\Sigma(1385)N$, $\Lambda(1405)N$, and $\bar{K}NN$ systems as well as the $\pi\Lambda N$ and $\pi\Sigma N$ systems, at the same time. This kind of study has never been done.

3. Inclusive Spectrum

The details of the analysis on the inclusive $d(\pi^+, K^+)X$ spectrum are described in Ref. [34]. Here, we show the inclusive missing-mass spectra of the $d(\pi^+, K^+)X$ reaction in the forward scattering angles between 2° and 16° in the laboratory system as double differential cross-sections,

$$\frac{d^2\bar{\sigma}(\theta_1 - \theta_2)}{d\Omega dM} = \frac{A}{N_A \rho x} \frac{N_{\pi K}}{N_{beam} \Delta\Omega(\theta_1 - \theta_2) \Delta M \times \epsilon}, \tag{1}$$

where A is the target mass number, N_A the Avogadro constant, ρx the target mass thickness, $N_{\pi K}$ the number of good (π^+, K^+) events in the missing-mass interval ΔM, N_{beam} the number of beam pions on the target, $\Delta\Omega(\theta_1 - \theta_2)$ the solid

angle of SKS between θ_1 and θ_2, and ϵ the overall experimental efficiency. In this analysis, the error of efficiency(ϵ) is expressed as the systematic uncertainty. The statistical error is negligibly small compared with the systematic one. In Table 1, the efficiencies commonly used for all the events are listed. The overall experimental efficiency ϵ is the product of these ϵ_{com} and the efficiencies corrected event-by-event such as the tracking efficiency in the SKS spectrometer($\epsilon_{SKStrack}$), K^+ decay factor(f_{decay}), vertex cut efficiency(ϵ_{vertex}) and the acceptance of the SKS(ϵ_{Acc}) as,

$$\epsilon = \epsilon_{com} \times \epsilon_{SKStrack} \times f_{decay} \times \epsilon_{vertex} \times \epsilon_{Acc}. \tag{2}$$

A typical value of $\epsilon = 17.6 \pm 0.7(syst)\%$ is obtained with an error $\Delta\epsilon/\epsilon = 4.4\%$. The SKS tracking efficiency was estimated with the (π^+, p) reaction data in which there is no decay in flight. Then, the effect of the K^+ decay in flight in the SKS magnet was corrected event-by-event, taking account of the flight path length and the kaon momentum. The resolution of the reaction vertex point depends on the scattering angle. In particular, the vertex resolution along the beam axis becomes very large for very small scattering angles. Therefore, the efficiency of the vertex cut was corrected for each event. The acceptance of the SKS spectrometer was estimated with a Monte Carlo simulation by using the magnetic field maps as a function of the missing mass and scattering angle.

Table 1: List of the experimental efficiency and systematic errors in the inclusive (π^+, K^+) reaction which are common for all the events.

Efficiency	Explanation	Typical value (%)	$\Delta\epsilon/\epsilon$ (%)
$\epsilon_{BeamTOF}$	Beam TOF efficiency	99.6 ± 0.1	0.1
$1 - f_\mu$	μ contamination factor	96.6 ± 0.1	0.1
ϵ_{BC12}	BC1-2 efficiency	93.8 ± 1.9	2.0
ϵ_{BC34}	BC3-4 efficiency	99.1 ± 0.1	0.1
$\epsilon_{K18Track}$	K1.8 tracking efficiency	87.9 ± 1.2	1.4
ϵ_{TOF}	TOF efficiency	99.5 ± 0.4	0.4
ϵ_{LC}	LC efficiency	99.6 ± 0.1	0.1
ϵ_{LAC}	LAC efficiency	93.3 ± 0.5	0.5
ϵ_{SDC12}	SDC1-2 efficiency	95.7 ± 1.7	1.8
ϵ_{SDC34}	SDC3-4 efficiency	99.2 ± 0.0	0.0
ϵ_{PID}	Particle ID efficiency for K^+	97.2 ± 0.7	0.7
ϵ_{DAQ}	Data Acquisition efficiency	65.7 ± 1.0	1.5
ϵ_{trig}	Trigger efficiency	91.6 ± 0.7	0.8
	Total	ϵ_{com} = 40.4 ± 1.5	3.6

The mass of the produced particle, $MM_d(MM_p)$, in the $d(\pi^+, K^+)X$ reaction is obtained as a missing mass expressed using the following equation in the laboratory frame

$$MM_d(MM_p) = \sqrt{\{E_\pi + M_d(M_p) - E_K\}^2 - \{p_\pi^2 + p_K^2 - 2p_\pi \cdot p_K \cos\theta_{\pi K}\}}, \tag{3}$$

where E_π and p_π are the total energy and momentum of a pion, E_K and p_K are those of a kaon, $M_d(M_p)$ is the deuteron(proton) rest mass, and $\theta_{\pi K}$ is the scattering angle of the reaction. Three kinematic variables, p_π, p_K and $\theta_{\pi K}$, are obtained through the momentum reconstruction in the spectrometers event by event.

In Fig. 4, the missing-mass spectrum of the $d(\pi^+, K^+)$ reaction at 1.69 GeV/c in the laboratory scattering angles between 2° and 16° is shown in the missing-mass scale of MM_d. As expected, we can find three major structures: quasi-free Λ production, quasi-free Σ^+ and Σ^0 productions, and quasi-free Y^* ($\Lambda(1405)$, $\Sigma^*(1385)^+$, and $\Sigma^*(1385)^0$) productions. In this spectrum, the three Y^* contributions are overlapped due to their intrinsic widths and nucleon Fermi motion. There are some contributions of non-resonant phase space components of $K^+\Lambda\pi$ and $K^+\Sigma\pi$ under the quasi-free Y^* bump.

The absolute momentum scale of the missing-mass measurement was adjusted using several calibration data, momentum matching between the two spectrometers for the 0.9 GeV/c beam, and the Σ^+ mass in the $p(\pi^+, K^+)$ reactions at two incident momenta at 1.58 and 1.69 GeV/c. We estimated that the uncertainty of the momentum scale

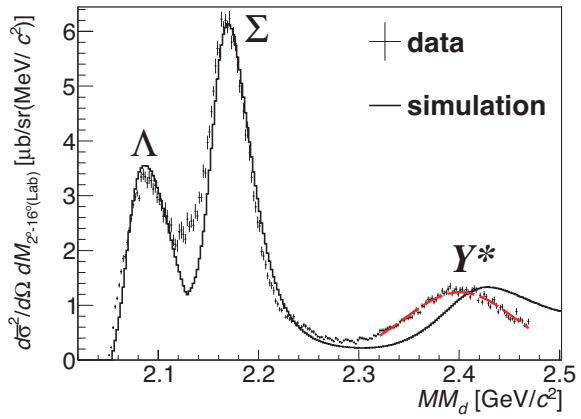

Figure 4: The missing-mass spectrum (MM_d) of the $d(\pi^+, K^+)$ reaction at 1.69 GeV/c for the scattering angle from 2° to 16° (Lab). The crosses show the data and a solid line shows a simulated spectrum assuming quasi-free kinematics. The red-dashed curve shows a result of the Y^* peak fitting for the present data. (Taken from Ref. [34])

was ±1.1 MeV/c. It was also confirmed that our missing-mass measurement gave us a known $\Sigma^*(1385)$ mass and width in the $\pi^+ + p \rightarrow K^+ + \Sigma(1385)^+$ reaction at 1.69 GeV/c, which were found to be 1381.1 ± 3.6($stat$) MeV/c^2 and 42 ± 13($stat$) MeV, respectively. The production cross-sections in the forward angles of the $p(\pi^+, K^+)\Sigma^+$ at 1.58 and 1.69 GeV/c and $p(\pi^+, K^+)\Sigma(1385)^+$ were compared with the previous measurements, and we confirmed they were consistent within the large statistical errors in the old measurements [34].

We made an attempt to reproduce the double differential cross-section $d^2\sigma/d\Omega dM$ with a Monte Carlo simulation by using the differential cross-sections $d\sigma/d\Omega$ of each elementary reaction obtained in past experiments [31, 35, 36] with a smearing by the nucleon Fermi motion in a deuteron. Here we used the cross-sections of the $\pi^- p \rightarrow K^0 X$ reaction assuming isospin symmetry for the $\pi^+ n \rightarrow K^+ X$ reaction. We assumed there is no rescattering of any of the final state particles such as K^+, hyperons, Y^*s etc. Here, we used a deuteron wave-function(Fig. 5-(Top)) derived from the Bonn potential [37].

In this simulation, the participant nucleon mass, $M^*{}_p$, was assumed to be off-shell by taking into account the Fermi motion, p_F, as:

$$M_p^{*2} = \left(M_d - \sqrt{M_s^2 + p_F^2}\right)^2 - p_F^2, \tag{4}$$

where M_d and M_s are deuteron and spectator on-shell nucleon mass, respectively (spectator model [38]). The emitted K^+ momentum, p_K, was distributed according to the reaction kinematics with the mass of the participant nucleon $M^*{}_p$ and its momentum $\vec{p}$. Then, the missing mass MM_d was calculated as $MM_d^2=(E_\pi + M_d - E_K)^2 - |\vec{p}_\pi - \vec{p}_K|^2$.

The result is shown in Fig. 4 as a solid line. An overall structure is rather well reproduced with this simple simulation. However, at the missing-mass of 2.13 GeV/c^2, which is the threshold for the ΣN channel, a difference was observed due to the cusp effect. When we selected the forward scattering angle of $\theta_{\pi K} < 8^\circ$, the clear structure due to the ΣN cusp was observed [34]. Further, the peak position for the quasi-free Y^* bump was shifted by approximately 30 MeV/c^2 toward the low-mass side in the MM_d scale. When we fitted the bump with a Gaussian function, we obtained the peak position at 2400.6 ± 0.5($stat$) ± 0.6($syst$) MeV/c^2 for the present data and at $2433.0^{+2.8}_{-1.6}$($syst$) MeV/c^2 for the simulation as shown in Fig. 4. The systematic error for the simulation was estimated by considering the uncertainties of the Y^* production cross-sections, Y^* mass, and fitting ranges. The same fitting procedure was applied to the data in the MM_p scale. We found a Y^* peak shift of $32.4 \pm 0.5(stat)^{+2.9}_{-1.7}(syst)$ MeV/c^2($22.4 \pm 0.4(stat)^{+2.7}_{-1.7}(syst)$ MeV/c^2) for the $MM_d(MM_p)$ spectrum toward the low-mass side.

In Fig. 5, the differential cross-sections used in the simulation are plotted in the center-of-mass frame. They are based on the results of the Legendre fit in the references if available. Exceptions are the cases for $\pi^+ p \rightarrow K^+\Sigma^+$ and $\pi^+ p \rightarrow K^+\Sigma(1385)^+$: we performed the fits to the data in Ref. [35, 36]. In the case of three-body reactions such as $\pi + n \rightarrow K^+\Lambda\pi$, final state particles are distributed in a three-body phase space. In the case of the Σ^0 production,

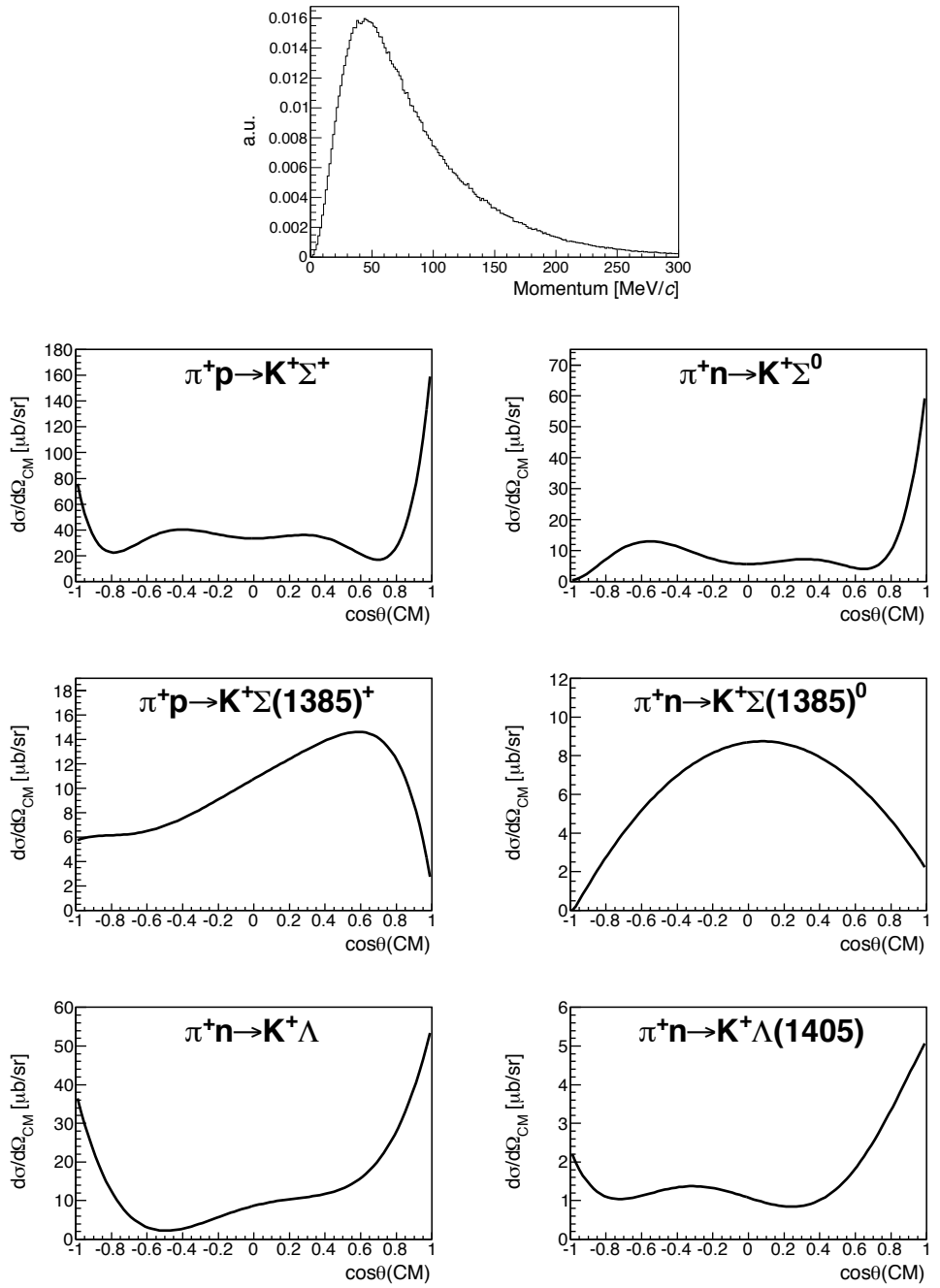

Figure 5: (Top) Momentum distribution of a nucleon in a deuteron obtained from the Bonn potential [37]. (Bottom) Differential cross-sections of the two-body reactions of hyperon ($\Lambda, \Sigma^{+,0}$) and hyperon resonance ($\Lambda(1405), \Sigma(1385)^{+,0}$) productions at a pion incident momentum of 1.69 GeV/c in the center-of-mass frame.

the existing data have rather large errors in the forward scattering angles. Therefore, a normalization adjustment was performed for the quasi-free Σ component within the measurement errors.

Here it should be noted that the angular distribution of the Λ(1405) production is forward peaked, as are other hyperon (Λ and Σ) production processes. On the other hand, the angular distribution of the Σ(1385) production drops rapidly in the forward angles; it is not exactly zero at zero degrees, but is strongly suppressed, probably due to its spin-parity.

In Fig. 6, the missing-mass spectra are sliced in two-degree steps in order to check the shifts of the Y^* bump at different angles. We can find that the large shift of ∼20 MeV exists at every angle. The peak positions are plotted in Fig. 6-(Bottom). As for the simulation, the peak position moves slightly from 1403 MeV/c^2 to 1397 MeV/c^2 because the contribution of the Λ(1405) is dominant at these highly forward directions and the Σ(1385) contribution increases as the scattering angle increases, as mentioned above. However, the data do not show such a trend.

In any case, the shift should be attributed to Σ(1385) because of the production cross-section dominance at these scattering angles, except for the very forward angles of 2-4 degrees, where we might need to consider the Λ(1405) contribution. As we discussed in Sec. 1, it seems that the situation is qualitatively similar to that found for the Δ resonance. In fact, there is a measurement of the invariant mass of the Σ(1385) with the $\Lambda + \pi^+$ decay mode in the $\pi^+ d \to K^+\Lambda\pi^+(n_s)$ reactions at incident beam momenta between 1.1 and 2.4 GeV/c [39]. The measured mass and width of 1386.6 ± 4.4 MeV/c^2 and 49 ± 11 MeV, respectively, are consistent with the known values in vacuum; namely there is no shift in the quasi-free Σ(1385) production in deuteron. Perhaps, $\Sigma(1385)N \to YN$ conversions might contribute to the observed shift. In addition, the SPring-8/LEPS collaboration measured an inclusive missing-mass spectrum of the $d(\gamma, K^+\pi^-)X$ reaction at a 1.5-2.4 GeV incident photon energy [19]. The collaboration was able to reproduce the obtained spectrum with quasi-free hyperon or hyperon resonance processes, whose yields were treated as free parameters.

Since we still have a shift at the very forward angles, the contribution to the shift from the Λ(1405) cannot be omitted. In any case, a possible unambiguous signal of the "K^-pp" production at around 2.27 GeV/c^2 is hardly visible in the inclusive spectrum.

4. Coincidence Analysis

Surrounding the target from 39° to 122° (Lab), we installed a range counter system as shown in Fig. 7-(a). There were six range counter arrays (RCAs), each having five layers of plastic scintillation counters of thicknesses 1 cm, 2 cm, 2 cm, 5 cm, and 2 cm. Protons were well separated from pions as shown in Fig. 7-(b) by using the range and time-of-flight information.

Among the five layers, in the case when particles stop in the first layer, the total energy deposit in the first layer and the velocity ($1/\beta$) were used for the particle identification. In the cases when particles stop in the second, third, and fourth layers, all the information of the velocity and range (energy deposits in the stop layer and one layer before the stop layer) were used. In the case when all the five layers have hits, pions with such high energy should have $\beta > 0.7$, while the maximum proton momentum from the K^-pp signal is 800 MeV/c ($\beta = 0.65$). Thus by applying the velocity cut $\beta < 0.65$ we can select protons separated by pions in such events.

The velocity of the particle (β) was measured from the time of flight between the first layer of the RCA and the BH2 trigger counter. The typical time resolution was 158 ± 16 ps. The vertical hit position along the RCA counter was obtained from the time difference between the two timings measured at both ends of a scintillator, and its resolution was approximately 8 mm in σ.

The detection efficiency of the RCAs for pions and protons was investigated with the $p(\pi^+, K^+)\Sigma^+$ reaction at 1.69 GeV/c. The production of Σ^+ was identified in the (π^+, K^+) missing mass, and the momentum and emission angle of the Σ^+ were obtained. We used the proton and π^+ from the Σ^+ decay ($\Sigma^+ \to p\pi^0$ or $\Sigma^+ \to n\pi^+$) for this study. The proton and π^+ were well separated only from the velocity information. As for the π^+, we obtained an RCA coincidence probability consistent with our simulation, which suggests we understood the geometrical acceptance of the RCAs reasonably well. On the other hand, for the proton, our simulation overestimated by approximately 20% the proton coincidence probability. Since the proton detection efficiency is strongly dependent on the incident angle to the RCA in the simulation, the difference might be due to the ambiguity in the incident angle distribution of protons.

The outline of the coincidence analysis is described in Ref. [40]. First, we required a coincidence of one proton with a momentum of ≥250 MeV/c in the middle of the RCA on each side (Seg. 2 and 5 in Fig. 7-(a)). According to our

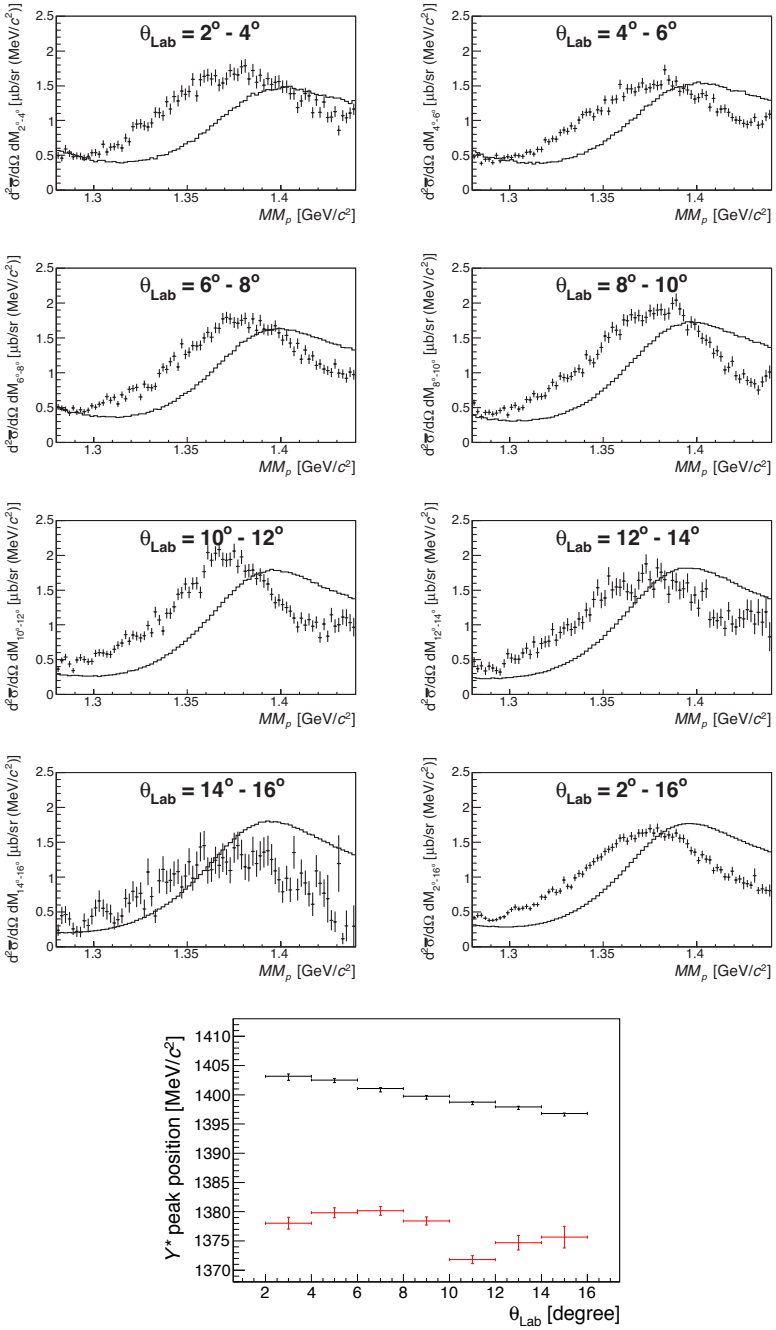

Figure 6: (Top) The double differential cross-sections (crosses) of the $\pi^+ + d \rightarrow K^+ + X$ reaction as a function of the missing-mass calculated in the kinematics of the proton as a target. They are plotted in each scattering angle range of two-degree step, compared with the simulated spectra (solid lines). (Bottom) Y^* peak positions in each two-degree slice for the present data (red, lower branch) and the simulation (black, upper branch) in the MM_p spectra.

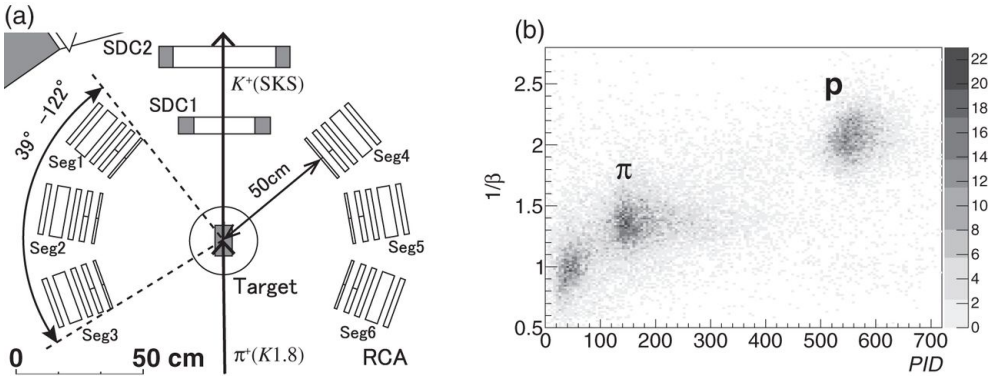

Figure 7: (a) Schematic view of the E27 range counter system [40]. (b) A scatter plot of a *PID* parameter and $1/\beta$, showing a good separation of protons and pions.

simulation, those quasi-free reactions observed in the inclusive spectrum rarely emit such a high-momentum proton in the angular coverage of the RCAs (Fig. 8-(a)). On the other hand, the protons from $K^-pp \to \Lambda p$, $\Lambda \to p + \pi^-$, hit the RCAs as shown in Fig. 8-(b).

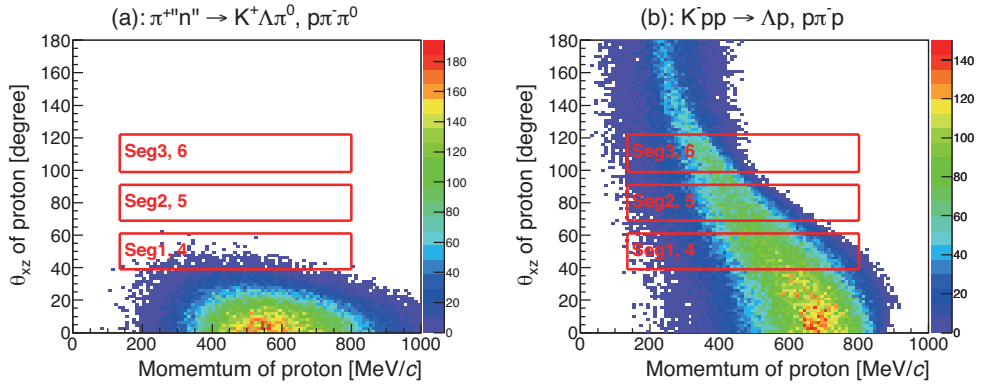

Figure 8: (a) Scatter plot between momentum and scattering angle in horizontal plane(xz) of protons emitted from a typical quasi-free process of π^+"n"$\to K^+\Lambda\pi^0$, $\Lambda \to p\pi^-$ in simulations. (b) Same scatter plot for the $K^-pp \to \Lambda p, \Lambda \to p\pi^-$ process. The acceptance for each segment of RCA is shown with red boxes.

Figure 9-(a) shows an inclusive MM_d spectrum without acceptance correction. The missing-mass spectrum with such a proton coincidence is shown in Fig. 9-(b). In this spectrum, there could be non-quasi-free contributions coming from the K^-pp signal decaying into $\Lambda(\Sigma^0)p$, such as threshold cusp background emitting through a strong conversion of $\Sigma^+n \to \Lambda p$, and backgrounds of quasi-free hyperons and hyperon resonance productions followed by conversion such as $\Sigma N \to \Lambda N$.

To contrast the contribution of each component, a ratio histogram between the one-proton coincidence spectrum and the inclusive one is presented in Fig. 9-(c), showing the proton coincidence probability as a function of the missing mass. There are two structures: one near the ΣN threshold cusp and the other at around 2.27 GeV/c^2. In the missing-mass region in between the two structures and in the quasi-free Y^* region the proton coincidence probability is smaller than the two prominent structures and stays rather constant. The broad bump structure at around 2.27 GeV/c^2 could be a signal of the "K^-pp".

As a comparison, the same coincidence plot for pions is shown in Fig. 10. According to our simulations, the pions from hyperon and hyperon resonance decays are easily detected with the RCAs, because they are widely emitted in

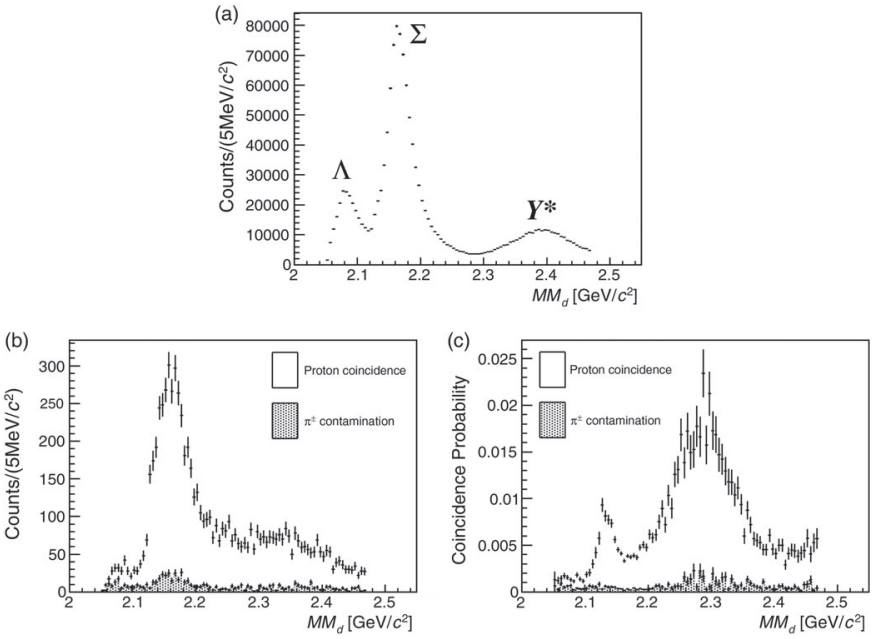

Figure 9: (a) The inclusive missing-mass spectrum of the $d(\pi^+, K^+)$ reaction at 1.69 GeV/c. (b) Missing-mass spectrum of the $d(\pi^+, K^+)$ reaction with one proton coincidence in the middle of the RCA on each side. (c) The coincidence probability of a proton obtained by dividing the coincidence spectrum (b) with the inclusive one (a). (Taken from Ref. [40])

the laboratory system due to the light pion mass. Therefore, the pion coincidence probability directly reflects the pion emission branch and the pion multiplicity in the final state for each quasi-free process: (I) quasi-free Λ production, (II) quasi-free Σ production, and (III) quasi-free Y^* production processes. For example, $\Sigma(1385)^+$ mainly decays as $\Sigma(1385)^+ \rightarrow \Lambda\pi^+ \rightarrow p\pi^-\pi^+$ (55.6%). On the other hand, Σ^+ can decay to $n\pi^+$(48.3%). Therefore, the pion coincidence probability of $\Sigma(1385)^+$ should be higher than that of Σ^+ because $\Sigma(1385)^+(\Sigma^+)$ can produce two(one) pions. Such a tendency can be observed in the obtained data in Fig. 10. Our simulation also explains the data well, while there exist slight differences in the Y^* region, which might be due to the observed Y^* shift and is not explained with our simple quasi-free simulation. Thus, the coincidence probability as the function of MM_d seems to be a valid analysis measure to investigate the reaction process involved.

In order to take into account the acceptance of our range counter system, we need information of the final state of the W in the $\pi^+ d \rightarrow K^+ W$ reaction. This study was carried out by requiring coincidence of two protons in the RCAs. In order to detect the two protons in our system, the final state of the W should be a) Λp, $\Lambda \rightarrow p\pi^-$, b) $\Sigma^0 p$, $\Sigma^0 \rightarrow \Lambda\gamma \rightarrow p\pi^-\gamma$, and c) $Y\pi p \rightarrow pp\pi\pi(\gamma)$, where Y is a hyperon such as Λ/Σ. We identified such a final state by determining the missing-mass squared spectra of X in the $d(\pi^+, K^+pp)X$ process by measuring the momenta of two protons in the decay of the ppX system of which the mass is MM_d. In this analysis, the absolute value of the proton momenta were obtained from the velocity and emission angles, estimated from the vertex position of the (π^+, K^+) reaction point and hit position of the first layer of the RCA. The first two modes, a) and b), are non-mesonic and the X is one pion (and γ). The last one, c), is mesonic and the X is two pions. Therefore, the missing-mass squared spectrum of ${M_X}^2$ should show a different distribution for each decay mode. Figure 11 shows such missing-mass squared spectra of ${M_X}^2$ for each MM_d region. The obtained data are indicated by black points with error bars. These points are shown after subtraction of the $\pi^\pm$ contamination fraction, whose distributions were almost flat in the ${M_X}^2$. The colored dashed-lines in Fig. 11 show the Λp, $\Sigma^0 p$, and $Y\pi p$ final-state components, whose normalization factors were adjusted in a template fit. The black lines in the figure are the sum of the three components.

These templates were obtained from the simulation, which assumed the reaction of $\pi^+ d \rightarrow K^+ W$, $W \rightarrow pY(pY\pi)$ with uniform productions in the center-of-mass frame. In the Λp and $\Sigma^0 p$ decay modes, we assumed uniform decay

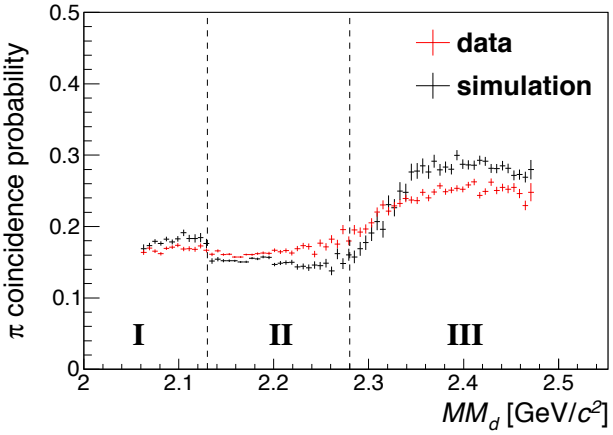

Figure 10: A comparison of the π coincidence probability spectra for the data (red) and simulation (black).

distributions in the center-of-mass system. The template for the $Y\pi p$ modes were produced by mixing the $\Sigma^+\pi^- p$, $\Sigma^0\pi^+ p$, and $\Lambda\pi^0 p$ components based on the elementary production cross-sections of Y^*s and their decay branches to $Y\pi$ modes. From the template fitting, we obtained the branching fraction into each decay mode for each MM_d and ${M_X}^2$.

The two-proton detection efficiency of the range counter system for each decay mode was estimated with a GEANT4-based Monte Carlo program, assuming uniform decay distribution in the center-of-mass frame of each MM_d. An example for the $\Sigma^0 p$ decay mode is shown in Fig. 12. It is almost flat in the missing-mass MM_d except near the production threshold. The efficiency was corrected event-by-event according to the MM_d and scattering angle $\theta_{\pi K}$.

Figure 13-(a) shows the missing-mass distribution of the $d(\pi^+, K^+)$ reaction in the $\Sigma^0 p$ decay mode after the mass-acceptance correction of the RCAs. Possible background sources of the two-proton coincidence events are non quasi-free processes or re-scattering in the deuteron. There are two categories of reactions: elastic and inelastic. The elastic processes include $\Lambda p \to \Lambda p$, $\Sigma^0 p \to \Sigma^0 p$, and $Y^* p \to Y^* p$. They do not contribute to the two-proton events because of the small Q-value according to our simulation. On the other hand, inelastic reactions with large Q-value, such as $\Sigma N \to \Lambda p$, $Y^* N \to YN$, etc. may contribute as backgrounds.

In Fig. 9-(c), the proton coincidence probability is very small below the ΣN threshold; it is reasonable because there is no background source in this MM_d region, only the $\Lambda N \to \Lambda N$ elastic scattering exists. However, the Λp decay mode in the MM_d region above the ΣN thresholds could be contaminated with the $\Sigma^+ n/\Sigma^0 p \to \Lambda p$ conversion process. On the other hand, there are no such background contributions in the $\Sigma^0 p$ decay mode below the $Y^* N$ production thresholds.

The spectrum was fitted with a relativistic Breit-Wigner function:

$$f(MM_d) = \frac{(2/\pi) MM_d m_0 \Gamma(q)}{(m_0^2 - MM_d^2)^2 + (m_0\Gamma(q))^2}. \tag{5}$$

The mass-dependent width was $\Gamma(q) = \Gamma_0(q/q_0)$, in which $q(q_0)$ is the momentum of the Σ^0 and proton in the $\Sigma^0 p$ rest frame at mass $MM_d(m_0)$. Note that we did not use the Λp spectrum for the evaluation of the mass and width of the "$K^- pp$"-like structure. The fit result is also shown in Fig. 13-(a) as a red curve. The mass and width were found to be 2275^{+17}_{-18}(stat.)$^{+21}_{-20}$(syst.) MeV/c^2 and 162^{+87}_{-45}(stat.)$^{+66}_{-78}$(syst.) MeV, respectively. This corresponds to the binding energy of the "$K^- pp$" system of 95^{+18}_{-17}(stat.)$^{+30}_{-21}$(syst.) MeV.

The largest systematic uncertainty was caused in the branching fraction determination in the template fitting of the ${M_X}^2$ spectra. We can estimate the branching fractions by using the missing-energy spectra (E_X) in a similar way. The errors on the mass and width were found to be 9 MeV/c^2 and 61 MeV, respectively. There are other sources of systematic errors, such as decay distribution and mixture of three different modes in estimating the $Y\pi p$ template, fitting functions other than Eq. 5, the spectrum binning and fitting range, and so on.

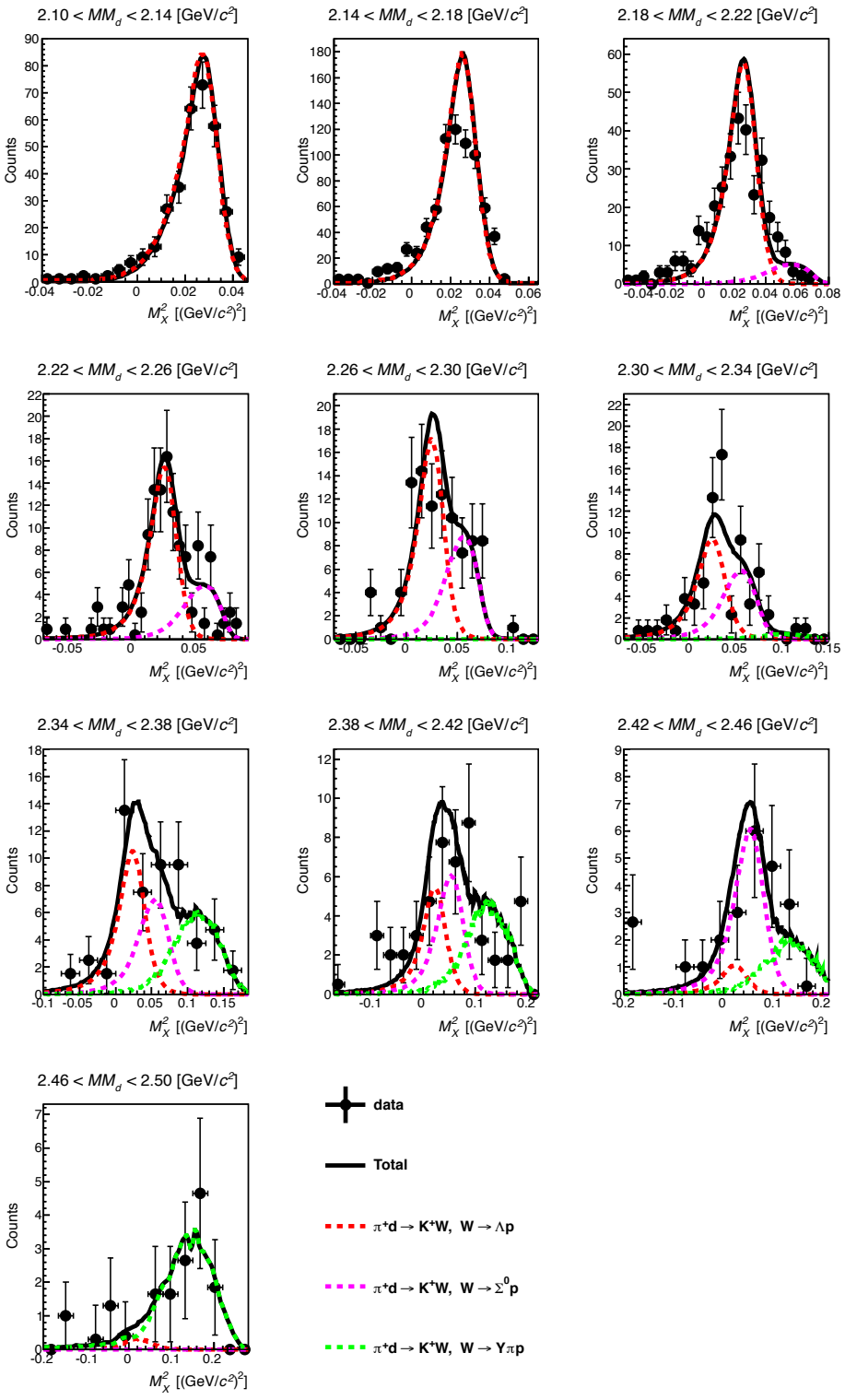

Figure 11: Missing-mass squared spectra of X in the $d(\pi^+, K^+pp)X$ reaction with two-proton coincidence. Each spectrum shows thespectrum for the different MM_d range shown in the figure. The spectra were fitted with three components of Λp (red dashed-line), $\Sigma^0 p$ (magenta dashed-line) and $Y\pi p$ (green dashed-line) modes.

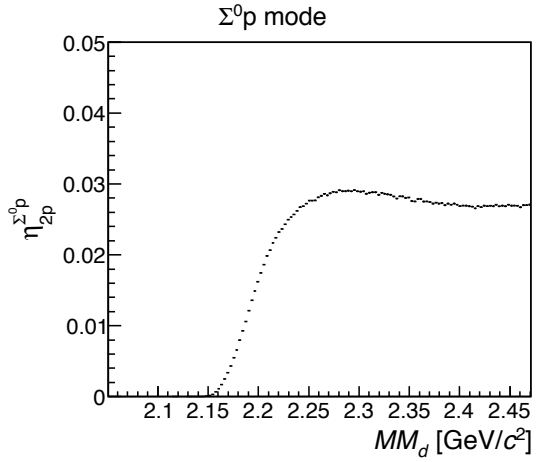

Figure 12: Detection efficiency of two protons in the range counter system as a function of the missing-mass, MM_d, which decays to $\Sigma^0 p$.

The production cross-section of the "$K^- pp$"-like structure decaying to $\Sigma^0 p$ was estimated from the fit of the $\Sigma^0 p$ spectrum by using the evaluated mass and width of the "$K^- pp$"-like structure. The evaluated production cross-section was $d\sigma/d\Omega_{K^- pp\to\Sigma^0 p} = 3.0 \pm 0.3(stat)^{+0.7}_{-1.1}(syst)$ μb/sr. The systematic errors of these values were estimated considering the uncertainties in the fitting ranges, the binning of the missing-mass spectrum, the detection efficiency of two protons in the RCA, and the Breit-Wigner shape. The differential cross-section of the "$K^- pp$"-like structure of the Λp decay mode was also estimated from the fitting assuming the same mass distribution of MM_d. Since there is a large enhancement due to the threshold cusp and $\Sigma N \to \Lambda p$ conversion, such a low-mass region was excluded from the fit. Thereby, the branching fraction of the "$K^- pp$"-like structure was obtained as $\Gamma_{\Lambda p}/\Gamma_{\Sigma^0 p} = 0.92^{+0.16}_{-0.14}(stat)^{+0.60}_{-0.42}(syst)$.

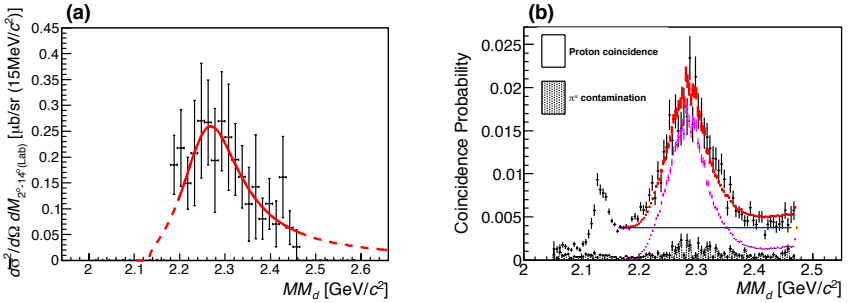

Figure 13: (a) The missing-mass spectrum of the $d(\pi^+, K^+)$ reaction for two-proton coincidence and the $\Sigma^0 p$ decay branch events. The curve overlaid corresponding to an example of the relativistic Breit-Wigner fit. (b) The coincidence probability of one proton in Fig. 9-(c) together with interpretation spectra (see the details in the text). (Taken from Ref. [40])

5. Discussion

First, we compare the production cross-section of the "$K^- pp$"-like structure with the known elementary cross-sections. The contribution of the Y^*'s production in the inclusive spectrum is evaluated to be $d\sigma/d\Omega_{Y^*} = 168.6 \pm 6.3$ μb/sr, and that of $\Lambda(1405)$ is found to be 36.9 ± 1.8 μb/sr [31]. Thus, the production ratios of the "$K^- pp$"-like structure, which decays to $\Sigma^0 p$ mode, compared with the Y^*s is $(d\sigma/d\Omega_{K^- pp\to\Sigma^0 p})/(d\sigma/d\Omega_{Y^*}) = 1.8 \pm 0.2(stat)^{+0.4}_{-0.7}(syst)\%$. The ratio compared with the $\Lambda(1405)$ production is $(d\sigma/d\Omega_{K^- pp\to\Sigma^0 p})/(d\sigma/d\Omega_{\Lambda(1405)}) = 8.2 \pm 1.0(stat)^{+1.9}_{-3.0}(syst)\%$. By

using the branching fraction of $\Gamma_{\Lambda p}/\Gamma_{\Sigma^0 p}$, the "$K^- pp$"-like structure production in the Λp decay mode amounts to 1.6% of the $d\sigma/d\Omega_{Y^*}$ and 7.5% of the $d\sigma/d\Omega_{\Lambda(1405)}$. By adding these two decay modes, we can evaluate the lower limit of the sticking probability of the $\Lambda(1405)p \to$ "$K^- pp$" reaction to be $\gtrsim$15.7%, where we assumed the "$K^- pp$"-like structure can be produced only form the $\Lambda(1405)$ doorway process. This lower limit of the sticking probability seems large compared with the theoretical value of approximately 1% [32].

By using the mass distribution for the "$K^- pp$"-like structure $f(MM_d)$ and the double differential cross-section of the inclusive (π^+, K^+) process, $\frac{d^2\sigma}{d\Omega dMM_d}(MM_d)_{Inclusive}$ shown in Fig. 4, we can obtain the coincidence probability spectrum as shown in Fig. 13-(a) as a plot colored in magenta, which is calculated as,

$$R_p(MM_d) = \frac{C \times f(MM_d) \times \eta_{1p}(MM_d)}{\frac{d^2\sigma}{d\Omega dMM_d}(MM_d)_{Inclusive}}, \tag{6}$$

where C is the normalization constant and $\eta_{1p}(MM_d)$ is the detection efficiency of a proton in the middle segments of the RCA (Seg2, 5) shown in Fig. 7-(a). The blue line in Fig. 13-(b) is an assumed flat component representing the conversion processes and the $\pi^\pm$ contamination due to the misidentification of $\pi^\pm$ in the RCA. Red points with error bars in Fig. 13-(b) are the sum of the magenta points and blue line. The normalization constant C and the amplitude of the flat component (blue line) were adjusted to minimize the differences between the black and red points. Thus, the obtained one proton coincidence probability spectrum of the broad enhanced region could be reproduced by the "$K^- pp$" signal and flat background.

The assumption of the flat component in the proton coincidence probability as a background would be a naive assumption considering that the re-scattering probabilities, such as $YN \to Y'N$ and $Y^*N \to YN$ are proportional to the products of the Y and Y^* fluxes (quasi-free production cross-sections) and their scattering cross-sections with another nucleon. If the scattering cross-sections have not such a large energy dependence in this energy region (typical Y and Y^* recoil momenta are 400-500 MeV/c) and if there is not such a large difference between Y and Y^*, the missing-mass distribution of the re-scattering probability would be proportional to the quasi-free production shape. Thus, the proton coincidence probability becomes nearly constant.

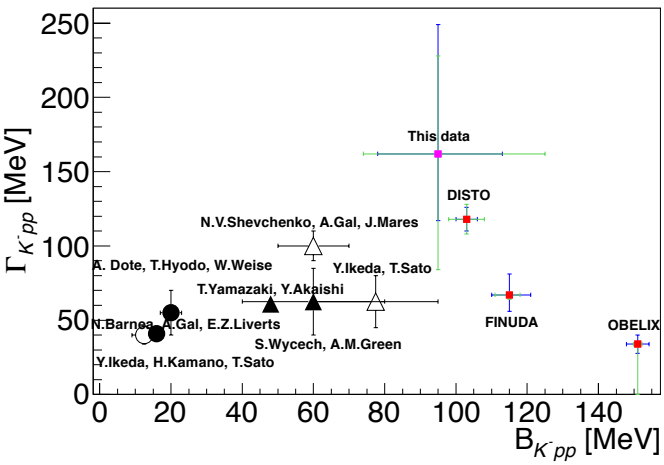

Figure 14: Comparison of the binding energy and width of the $K^- pp$. The calculated binding energy and width using the chiral SU(3)-based energy-dependent potentials are plotted with circles and the ones calculated with the energy-independent potentials are plotted with triangles. The calculation results with the variational and Faddeev methods are shown with open and filled symbols, respectively. The experimental values reported from the FINUDA [13], DISTO [14], and OBELIX [18] collaborations are shown together with the present result in red squares, where the statistical and systematic errors are shown with blue and green lines, respectively.

The observed mass and width of the "$K^- pp$"-like structure are compared with previous experimental values reported from the FINUDA collaboration [13] and the DISTO collaboration [14] together with several theoretical results [11] in Fig. 14. These binding energies reported in the experiments are approximately 100 MeV and larger

than any theoretical calculations. Compared with the difference in the binding energy, the difference in the width is relatively small; they agree each other at approximately 40-100 MeV, while in the theoretical calculations mainly the decay width into the $\pi\Sigma N$ channel is considered and the non-mesonic branch ($K^- pp \rightarrow YN$) is omitted.

This discrepancy in the binding energy is hard to explain in the "$K^- pp$" picture with the standard $\bar{K}N$ interaction. One idea is to attribute it to another picture of the $\pi\Sigma N$ channel. There is a theoretical suggestion [6, 41] that the pion-assisted $\pi\Lambda N - \pi\Sigma N$ dibaryon wth isospin and spin-parity $I(J^P)=\frac{3}{2}(2^+)$ appears near the $\pi\Sigma N$ threshold at $\sqrt{s} \approx 2270$ MeV. It is a strangeness $S = -1$ $N\Sigma(1385)$ dibaryon called $\mathcal{Y}_{\frac{3}{2}2}(2270)$. It will be produced as

$$\pi^+ + d \rightarrow \mathcal{Y}^+ + K^+, \;\; \mathcal{Y}^+ \rightarrow \Sigma^0 + p, \tag{7}$$

which is the detection mode in the present E27 experiment. Taking account of the production cross-section dominance of $\Sigma(1385)$ over $\Lambda(1405)$, this interpretation cannot be excluded. The isospin of $\frac{3}{2}$ for the $\mathcal{Y}$ can be examined with the specific reactions suggested in Ref. [6, 41]:

$$\pi^\pm + d \rightarrow \mathcal{Y}^{++/-} + K^{0/+}, \;\; \mathcal{Y}^{++/-} \rightarrow \Sigma^\pm + p(n). \tag{8}$$

The authors of Ref. [42] suggest that a $I(J^P) = \frac{1}{2}(0^-)$ πYN resonance appears near the $\pi\Sigma N$ threshold with a large decay width, which is similar to the case where the $\Lambda(1405)$ has a double pole structure in chiral $SU(3)$ models [43, 44]. This picture would also give a binding energy close to 100 MeV. There is another idea to explain the discrepancy by modifying the $\bar{K}N$ interaction in $K^- pp$. A theoretical calculation suggests that the enhancement of the $\bar{K}N$ attraction by ~20% could reproduce the $K^- pp$ binding energy [45].

6. Summary

The baryon number $B = 2$ and strangeness $S = -1$ systems were investigated by using the $\pi^+ + d \rightarrow K^+ + X$ reaction at the forward scattering angles $(2^\circ - 16^\circ)_{Lab}$ and the incident momentum of 1.69 GeV/c. The energy region from the ΛN threshold over the Y^*N region were covered with a large momentum acceptance spectrometer. The major contributions of the quasi-free Λ, Σ, and Y^*s ($\Sigma(1385)$ and $\Lambda(1405)$) processes were clearly observed. There were no Λp and ΣN bound state peaks. However, at the ΣN threshold at 2.13 GeV/c^2 a threshold cusp structure was observed. Another interesting observation was a shift of the quasi-free Y^* bump structure by approximately 30 MeV compared with a simple quasi-free simulation. From the angular dependence of the production cross-sections of the $\Sigma(1385)$ and $\Lambda(1405)$ in the forward angles, the $\Sigma(1385)$ must, at least, contribute to this shift. Further, the $\Lambda(1405)$ contribution at the very forward angles should not be neglected. It should be noted that similar shifts of quasi-free bump structure were observed for Δ productions in the (^{3}He, t) and (p, n) reactions.

In the $d(\pi^+, K^+)$ reaction, the $\Lambda(1405)$ production is suggested to act as a doorway to the formation of $K^- pp$ through $\Lambda^* p \rightarrow K^- pp$. It is a merit of the (π^+, K^+) reaction that the angular distribution shows the forward peaking in this angular range, while there is a drawback that the sticking probability would not be large because of the large recoil momentum of the $\Lambda(1405)$. In order to enhance the signal ("$K^- pp$" production) to noise (quasi-free $\Lambda(1405)$ production) ratio, proton(s) coincidence in a wide emission angle ($39^\circ - 122^\circ_{Lab}$) was required in the present experiment. In this analysis, we observed a large proton emission probability at around 2.27 GeV/c^2. From the obtained missing-mass distribution corresponding to the $\Sigma^0 p$ decay mode, the mass and width of the "$K^- pp$"-like structure were found to be $2275^{+17}_{-18}(stat)^{+21}_{-30}(syst)$ MeV/c^2 and $162^{+87}_{-45}(stat)^{+66}_{-78}(syst)$ MeV, respectively. This corresponds to a binding energy of $95^{+18}_{-17}(stat)^{+30}_{-21}(syst)$ MeV. The observed binding energy is larger than the theoretical calculations using the standard $\bar{K}N$ interaction models. It was suggested that a possible modification of the $\bar{K}N$ interaction by approximately 20% might explain it. Alternatively if we take the $\pi\Sigma N$ as the configuration, a state near the $\pi\Sigma N$ threshold is suggested. Such a picture could also explain the large binding energy of ≈100 MeV.

Acknowledgements

The author would like to thank all the collaborators in the J-PARC E27 experiment: Y. Ichikawa, H. Fujioka, H.C. Bhang, S. Bufalino, H. Ekawa, P. Evtoukhovitch, A. Feliciello, S. Hasegawa, S. Hayakawa, R. Honda, K. Hosomi, K. Imai, S. Ishimoto, C. Joo, S. Kanatsuki, R. Kiuchi, T. Koike, H. Kumawat, Y. Matsumoto, K. Miwa,

M. Moritsu, M. Naruki, M. Niiyama, Y. Nozawa, R. Ota, A. Sakaguchi, H. Sako, V. Samoilov, S. Sato, K. Shirotori, H. Sugimura, S. Suzuki, T. Takahashi, T.N. Takahashi, H. Tamura, T. Takana, K. Tanida, A.O. Tokiyasu, Z. Tsamalaidze, B. Roy, M. Ukai, T.O. Yamamoto, and S. Yang. This work is partially supported by MEXT KAKENHI Grant Number 17070005.

References

[1] D.H. Davis, *Nucl. Phys. A* **754** (2005) 3.
[2] M. May *et al.*, *Phys. Rev. C* **25** (1982) 1079.
[3] T. Nagae *et al.*, *Phys. Rev. Lett.* **80** 1605.
[4] T. Harada, *Phys. Rev. Lett.* **81** (1998) 5287.
[5] T. Harada, *Nucl. Phys. A* **672** (2000) 181.
[6] H. Garcilazo and A. Gal, *Nucl. Phys. A* **897** (2013) 167.
[7] K. Moriya *et al.*, *Phys. Rev. Lett.* **112** (2014) 082004.
[8] J.M.M. Hall *et al.*, *Phys. Rev. Lett.* **114** (2015) 132002.
[9] T. Uchino, T. Hyodo, M. Oka, *Nucl. Phys. A* **868-869** (2011) 53.
[10] Y. Akaishi and T. Yamazaki, *Phys. Rev. C* **65** (2002) 044005.
[11] For the recent theoretical status, please refer to A. Gal, *Nucl. Phys. A* **914** (2013) 270, and references therein.
[12] T. Nagae, Proc. of the HYP2015 conference, Sendai, Japan, 2015, to be published in *JPS Conf. Proc.*.
[13] M. Agnello *et al.*, *Phys. Rev. Lett.* **94** (2005) 212303.
[14] T. Yamazaki *et al.*, *Phys. Rev. Lett.* **104** (2010) 132502.
[15] P. Kienle *et al.*, *Eur. Phys. J. A* **48** (2012) 183.
[16] G. Agakishiev *et al.*, *Phys. Lett. B* **742** (2015) 242.
[17] G. Bendiscioli *et al.*, *Nucl. Phys. A* **789** (2007) 222.
[18] G. Bendiscioli *et al.*, *Eur. Phys. J. A* **40** (2009) 11.
[19] A.O. Tokiyasu *et al.*, *Phys. Lett. B* **728** (2014) 616.
[20] T. Hashimoto *et al.*, *Prog. Theor. Exp. Phys.* **2015**, 061D01.
[21] E. Oset, H. Toki, and W. Weise, *Phys. Rep.* **83** (1982) 281.
[22] C. Gaarde, *Ann. Rev. Nucl. Part. Sci.* **41** (1991) 187.
[23] T. Nagae *et al.*, *Phys. Lett. B* **191** (1987) 31.
[24] T. Udagawa, P. Otmanns, F. Osterfeld, S.W. Hong, *Phys. Rev. C* **49** (1994) 3162.
[25] B. Körfgen, F. Osterfeld, T. Udagawa, *Phys. Rev. C* **50** (1994) 1637.
[26] A. Gal and H. Garcilazo, *Phys. Rev. Lett.* **111** (2013) 170301.
[27] A. Gal and H. Garcilazo, *Nucl. Phys. A* **928** (2014) 73.
[28] P. Adlarson *et al.*, *Phys. Rev. Lett.* **106** (2011) 242302.
[29] P. Adlarson *et al.*, *Phys. Lett. B* **721** (2013) 229.
[30] T. Takahashi *et al.*, *Prog. Theor. Exp. Phys.* **2012**, 02B010.
[31] D.W. Thomas *et al.*, *Nucl. Phys.* **B56** (1973) 15.
[32] T. Yamazaki and Y. Akaishi, *Phys. Rev. C* **76** (2007) 045201.
[33] Y. Ichikawa *et al.*, Proc. 2nd Int. Symp. Science at J-PARC, JPS Conf. Proc. **8** (2015) 021020.
[34] Y. Ichikawa *et al.*, *Prog. Theor. Exp. Phys.* **2014**, 101D03.
[35] Y.-L. Pan and F.L. Forman, *Nucl. Phys.* **B21** (1970) 395.
[36] Y.-L. Pan *et al.*, *Phys. Rev. D* **2** (1970) 449.
[37] R. Machleidt, K. Holinde and Ch. Elster, *Phys. Rep.* **149** (1987) 1.
[38] M. Abdel-Bary *et al.*, *Eur. Phys. J. A* **29** (2006) 353.
[39] D.W. Davies *et al.*, *Phys. Rev. D* **2** (1970) 506.
[40] Y. Ichikawa *et al.*, *Prog. Theor. Exp. Phys.* **2015**, 021D01.
[41] A. Gal, *Acta Physica Polonica B* **47** (2016) 471.
[42] A. Dote, T. Inoue, and T. Myo, *Prog. Theor. Exp. Phys.* **2015**, 043D02.
[43] A. Dote, and T. Myo, *Nucl. Phys. A* **930** (2014) 86.
[44] Y. Ikeda, H. Kamano, and T. Sato, *Prog. Theor. Phys.* **124** (2010) 533.
[45] S. Maeda, Y. Akaishi, and T. Yamazaki, *Proc. Jpn. Acad., Ser. B* **89** (2013) 418.